CSIRO PUBLISHING
www.publish.csiro.au/journals/ijwf *International Journal of Wildland Fire* **2011**, *20*, 91–103

A North American regional reanalysis climatology of the Haines Index

Wei Lu[A,B], *Joseph J. Charney*[C,D], *Sharon Zhong*[B], *Xindi Bian*[C] *and Shuhua Liu*[A]

[A]Department of Atmospheric Sciences, School of Physics, Peking University, Beijing, 100871, P. R. China.
[B]Department of Geography, Michigan State University, East Lansing, MI 48823, USA.
[C]USDA Forest Service, 1407 South Harrison Road, Suite 220, East Lansing, MI 48823, USA.
[D]Corresponding author. Email: jcharney@fs.fed.us

Abstract. A warm-season (May through October) Haines Index climatology is derived using 32-km regional reanalysis temperature and humidity data from 1980 to 2007. We compute lapse rates, dewpoint depressions, Haines Index factors A and B, and values for each of the low-, mid- and high-elevation variants of the Haines Index. Statistical techniques are used to investigate the spatial and temporal variability of the index across North America. The new climatology is compared with a previous climatology derived from 2.5° (~280 km) global reanalysis data. Maps from the two climatologies are found to be very similar for most of North America. The largest differences appear along the eastern coastline and in regions of large elevation gradients, where the orography in the 32-km climatology is better resolved than that of the 2.5° climatology. In coastal areas of eastern North America and where there is steeply sloping terrain, the new climatology can augment the information from the 2.5° climatology to help analyse the performance and interpret the results of the Haines Index in these regions. A linear trend analysis of the total number of high-Haines Index days occurring in each warm season reveals no significant linear trends over the 28-year data period.

Additional keywords: fire climate, fire-weather forecasting, NARR.

Introduction

The Haines Index (HI), initially named the 'Lower Atmospheric Severity Index', is a widely used fire weather index that is formulated to detect the potential for a plume-dominated fire to become large or exhibit erratic fire behaviour (Haines 1988). Conceptually, the HI consists of an empirical relationship between a dry, unstable atmospheric layer and certain types of fire behaviour in large wildfires. The index is the combination of a lower-atmospheric stability term (factor A) and a moisture term (factor B) into a single number that is associated with observations of dangerous fire behaviour. Since its development, the HI has become widely used and accepted by fire managers as an indicator of the potential for an existing wildfire to become difficult to fight (Potter and Martin 2001). The HI is a standard element of US National Weather Service fire weather forecasts and is routinely employed as a planning tool for daily fire management activities.

The HI is computed by adding factor A and factor B. Factor A is determined by calculating the atmospheric lapse rate between two fixed pressure levels and factor B is determined from a dewpoint depression at a single pressure level. Each factor is assigned a number from 1 to 3 according to predetermined thresholds, and the two factors are summed with equal weighting. The pressure levels and thresholds used to calculate the HI are shown in Table 1. The resulting HI varies from 2, which is defined as a very low potential for wildfires to become large and erratic, to 6, which represents a very high potential (Haines 1988). As the HI employs fixed pressure levels in the lower troposphere to calculate factor A and factor B, the surface elevation at the location where the HI is computed must be considered. Haines (1988) employed United States climatological divisions to establish locations where low-, mid- and high-elevation variants of the HI were considered most appropriate, based on a subjective analysis of the elevation above mean sea level of each climate division. As the elevation above mean sea level at the boundaries between the climate divisions is not constant, the distribution of HI variants recommended by Haines (1988) is not tied to a specific surface elevation and therefore does not produce a spatially continuous continent-scale map of the HI using a gridded analysis. In order to calculate the HI using gridded meteorological data, it is necessary either to define elevation thresholds for transitions between the three HI variants, or to generate separate maps for each variant. Appendix 1 in Winkler *et al.* (2007) provides a comprehensive description of the calculation and interpretation of the HI.

Although fire weather forecasters and fire managers most often employ the HI locally to aid in making decisions regarding daily fire activities, several studies have expressed a need to understand the regional, continental and climatological behaviour and variability of the index (Werth and Werth 1998; Croft *et al.* 2001; McCaw *et al.* 2007). The most effective means of calculating the HI, including which variant of the HI and what

 10.1071/WF08196 1049-8001/11/010091

Table 1. Calculating the Haines Index (from Haines 1988)

Elevation	A		B	
	Calculation	Categories	Calculation	Categories
Low	950-hPa temperature minus 850-hPa temperature	A = 1 if <4°C A = 2 if 4 to 7°C A = 3 if ≥8°C	850-hPa temperature minus 850-hPa dew point	B = 1 if <6°C B = 2 if 6 to 9°C B = 3 if ≥10°C
Middle	850-hPa temperature minus 700-hPa temperature	A = 1 if <6°C A = 2 if 6 to 10°C A = 3 if ≥11°C	850-hPa temperature minus 850-hPa dew point	B = 1 if <6°C B = 2 if 6 to 12°C B = 3 if ≥13°C
High	700-hPa temperature minus 500-hPa temperature	A = 1 if <18°C A = 2 if 18 to 21°C A = 3 if ≥22°C	700-hPa temperature minus 700-hPa dew point	B = 1 if <15°C B = 2 if 15 to 20°C B = 3 if ≥21°C

observation time should be used at a given location, has also been discussed (Werth and Werth 1998; Croft *et al.* 2001; Potter *et al.* 2005). A climatological analysis provides a starting point from which researchers and operational users of the HI can attempt to determine whether they should adjust their methods of calculating and interpreting the HI at a given location (Potter *et al.* 2002).

Although several regional HI climatologies using station data have appeared in the literature over the last 10 years (Jones and Maxwell 1998; Werth and Werth 1998; Croft *et al.* 2001), the first comprehensive long-term climatology using continuous, gridded meteorological fields to calculate the HI appeared in Winkler *et al.* (2007) (hereafter referred to as the Winkler Haines Climatology or WHC). WHC employed 40 years of global reanalysis data (Kalnay *et al.* 1996; Kistler *et al.* 2001) developed by the National Centers for Environmental Prediction (NCEP) and the National Center for Atmospheric Research (NCAR) to analyse broad spatial and temporal trends in the HI for North America. Although the NCEP–NCAR global reanalysis (hereafter referred to as GR for brevity) employed by WHC identified broad climatological patterns in HI variation across North America, a higher-resolution gridded analysis could potentially enhance the ability of fire weather forecasters and fire managers to utilise a HI climatology for their local area.

In this paper, we employ the North American Regional Reanalysis (NARR) (Mesinger *et al.* 2006) to produce a higher-spatial-resolution HI climatology for North America. We hypothesise that a HI climatology computed from the NARR will resolve the impact of mesoscale variations in lapse rate and dewpoint depression on the continental and regional distribution of the HI, and in doing so provide fire managers and fire weather forecasters with additional climatological information that can be used to help interpret the HI at a given location in North America.

Data and methods

WHC chose to employ gridded reanalysis fields instead of the original radiosonde observations to produce a HI climatology because of the greater and more uniform spatial coverage of reanalysis fields, and owing to concerns about the quality of the radiosonde data. The large number of discontinuities in radiosonde time series at individual stations due to station relocations and changes in sensors can make the radiosonde record difficult to use for climatological analysis. WHC limited their analysis to 0000 hours (UTC), as this is the time period for which the HI was originally developed and its performance validated. The GR data employed by WHC consists of 6-hourly meteorological fields on a 2.5°-latitude by 2.5°-longitude grid with 28 vertical levels (Kalnay *et al.* 1996).

The meteorological data employed in this study were obtained from the NARR, which is a long-term, dynamically consistent, data-assimilation-based suite of climate data for North America (Mesinger *et al.* 2006) starting in 1979 and continuing to the present. The NARR improves on the earlier GR by employing additional types of meteorological observations, incorporating upgrades in operational NCEP regional models (e.g. Eta, the Weather Research and Forecasting (WRF) model) (Black 1988; Mesinger *et al.* 1988; Janjić 1994) and more advanced data-assimilation systems to increase the resolution and accuracy of the NARR compared with the GR. The NARR consists of 3-hourly meteorological data on a 32-km grid with 45 vertical levels. Mesinger *et al.* (2006) demonstrated that analyses of NARR precipitation fields over the continental United States compare favourably with observed precipitation distributions, and enhance the mesoscale detail in other meteorological fields that are affected by precipitation processes. Furthermore, NARR tropospheric temperatures and winds have been verified against rawinsonde observations, and 2-m temperatures and 10-m winds compared with surface station observations, achieving substantial improvements over the GR.

For this study, we generally follow the WHC methodology and employ temperature and humidity fields from a reanalysis product (the NARR) at 0000 hours (UTC) to produce a HI climatology. However, although WHC presented a combination of annual analyses and summer (June, July and August) analyses, we chose to perform all of our analysis on the May through October time period (which we will refer to as the 'warm season' hereafter, for brevity, with the understanding that at some locations, the warm season starts earlier and ends later). We chose this time period to enable a more direct comparison between results for all of the HI variants, as well as to include climatological conditions during the late spring and early autumn fire season in the northern United States and Canada. Furthermore, May through October corresponds more closely to the fire season for many mountainous areas in the western USA, where greater spatial variability is expected in lower tropospheric meteorological variables and the NARR-based HI climatology should have advantages over the GR-based WHC.

Although WHC employed GR data from 1961 to 2000, the NARR data used in this study span the 28-year period from 1980 to 2007. Our study area extends from 20 to 60°N latitude and 125 to 50°W longitude, covering most of North America except northern Canada and Western Alaska (see e.g. Fig. 1), which corresponds roughly to the study area in WHC. All of the NARR-derived quantities are presented in the form of spatial maps of this study area, with no smoothing or selective sampling of grid points applied to the graphical displays.

The HI and its factor A and factor B components are calculated at each reanalysis grid point. As discussed in the Introduction, Haines (1988) employed climatological divisions based on surface elevation to differentiate between low-, mid- and high-elevation variants of the HI. The WHC employed the same climatological divisions within the United States and 300- and 1000-m elevation contours in Canada and Mexico to differentiate between locations where the low-, mid- and high-elevation variants would be used. For our analysis, we chose to calculate each variant at every location where the pressure level (see Table 1) needed for the HI calculation is above the ground. This technique allows researchers and operational users to decide which HI variant (or variants) at a given location will be employed to determine whether they should adjust their methods of calculating and interpreting the HI.

The climatology includes not only mean HI values, but other statistical measures such as standard deviation and percentile classification, as computed in WHC. Frequencies and the maximum number of consecutive days in any year of HI ≥ 4, HI ≥ 5 and HI $= 6$ are computed to evaluate the occurrence and persistence of high HI values in the climatology. Finally, a simple linear regression in time (Variable X) for the number of days (Variable Y) in each warm season with HI ≥ 4 is computed. The slope (B) of the linear regression line ($Y = BX + A$), which indicates how much Y changes with a unit change in X, is used to assess the 28-year trend at each grid point. A test of the slope parameter (B coefficient) is conducted at each grid point to examine if it has a statistically significant relationship with Y. The coefficient of determination is also computed to indicate the fraction of the variance in the values of Y accounted for by time (X).

Results and discussion

Factor A – lower atmospheric stability

Maps of the warm-season climatological mean lapse rate (the quantity used to compute the HI factor A) are shown in Fig. 1. As noted above (Table 1), factor A, which represents the influence of the lower atmospheric stability on HI, can have values of 1, 2 or 3, dependent on the environmental lapse rate between two fixed pressure levels in the lower troposphere. In the east, where the low-elevation (950–850 hPa) variant is most commonly used, the lapse rates are smaller near the coast and increase towards the middle of the continent (Fig. 1*a*). The greatest spatial variability in the environmental lapse rates occurs in the west, in the mid- (850–700 hPa) (Fig. 1*b*) and high-elevation (700–500 hPa) (Fig. 1*c*) variants. A comparison with WHC indicates that the NARR is better at resolving the effect of the coastal plain and the Great Lakes on the mean low-elevation lapse rates than the GR used in WHC. Additionally, the

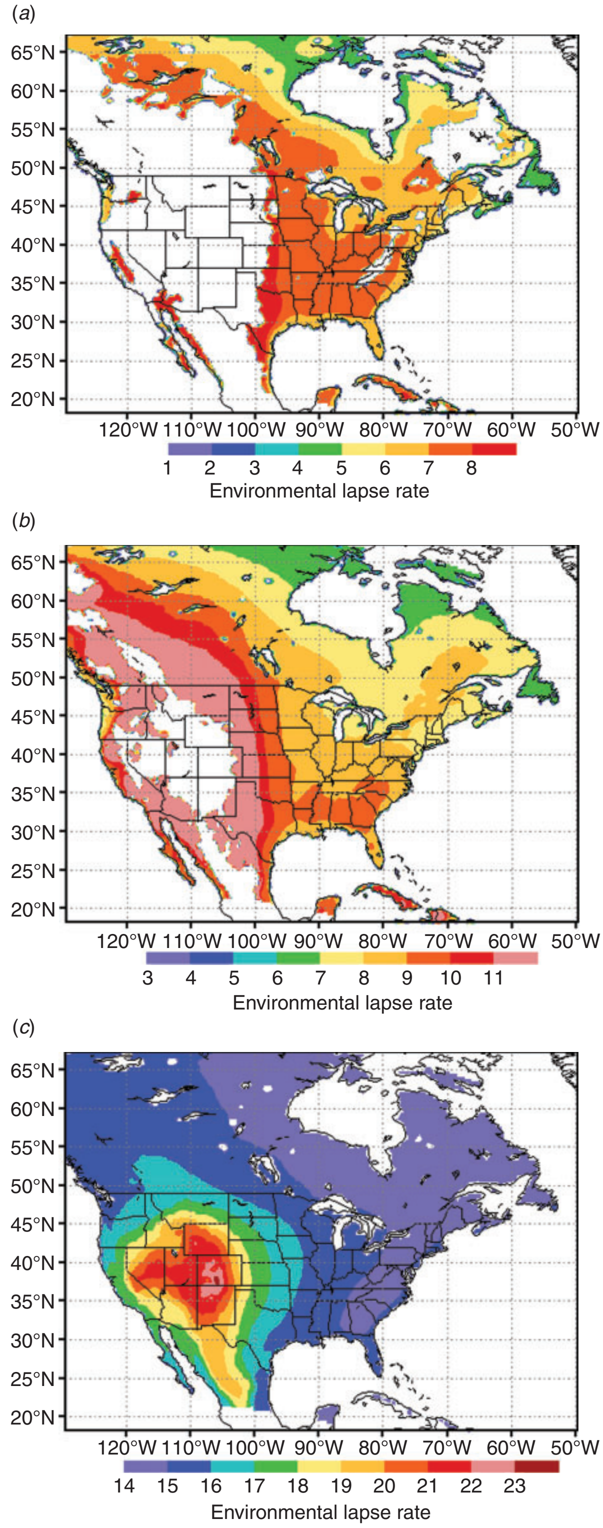

Fig. 1. Warm-season (May to October) mean environmental lapse rate (°C) during 1980–2007 for: (*a*) the low-elevation variant (950-hPa temperature minus 850-hPa temperature); (*b*) the mid-elevation variant (850-hPa temperature minus 700-hPa temperature); and (*c*) the high-elevation variant (700-hPa temperature minus 500-hPa temperature) of the Haines Index. Locations where surface pressure is less than the higher pressure in the range defined above are shown in white.

warm-season low-elevation mean lapse rates in the NARR are roughly 2°C km^{-1} larger than the annual mean values reported in WHC, although it is not entirely clear from this analysis whether this difference is due to the greater number of vertical levels in the NARR or due to the difference between the warm-season NARR and annual mean GR. As found in WHC, spatial variability in the mid-elevation lapse rate appears to be closely tied to orography in the east (Fig. 1*b*), although the NARR fields suggest that lapse rates are higher in the south-east United States away from the coastline and reveal spatial variability along the west coast of the United States that could not be presented by WHC owing to the comparatively coarse orography in the GR data. As in WHC, the mean high-elevation lapse rates exhibit considerable variability in the Intermountain West, with the largest values occurring near the Colorado–New Mexico border (Fig. 1*c*).

Maps of the warm-season climatological mean factor A for each of the three HI variants (Fig. 2) show less fine-scale detail than the corresponding mean lapse rate maps in Fig. 1. Specifically, the effects of the coastal plain and the Great Lakes on the low-elevation variant mean lapse rates (Fig. 1*a*) are not evident in the mean low-elevation factor A values (Fig. 2*a*). This result suggests that some of the meteorological variations resolved by the higher-resolution NARR data are smoothed by the calculation of factor A, most likely owing to the collapse of a large range of lapse rate values into only three integer values for factor A (Table 1). However, a strong dependence of the mid-elevation variant mean factor A (Fig. 2*b*) on increasing elevation in the Midwest is still evident, whereas complex structure appears at the boundary between 2 and 2.5 in the mean high-elevation factor A over the border between Colorado and New Mexico (Fig. 2*c*). So, whereas the calculation of factor A appears to generate smoother horizontal variations than those in the mean lapse rate maps at low elevations, at high elevations the smoothing is less pronounced.

Factor B – lower atmosphere moisture content

The HI factor B, representing the dryness of the atmosphere, assigns values of 1, 2 or 3 based on the magnitude of the dewpoint depression at a fixed pressure level. As with factor A, this choice of pressure level is dependent on topography, but unlike factor A, the same pressure level (850 hPa) is used for low- and mid-elevation variants. Only when computing the high-elevation variant does the factor B pressure level change (700 hPa). A map of the warm-season climatological mean dewpoint depression used in the low- and mid-elevation variants (Fig. 3*a*) shows the highest values in the west and the lowest values along the ridge of the Appalachians and in Florida. The NARR maps differ considerably from the WHC results, in that WHC shows the highest mean dewpoint depressions in the south and south-east, decreasing to the north, whereas the NARR shows higher values in the Midwest, decreasing to the east. The NARR resolves an east–west-oriented lobe of high 850-hPa mean dewpoint depressions along the Iowa–Missouri border into Illinois, a narrow band of low mean 850-hPa dewpoint depressions in eastern Texas, high mean 850-hPa dewpoint depressions in California, and lower mean 850-hPa dewpoint depressions in western Washington and central Oregon. None of these features

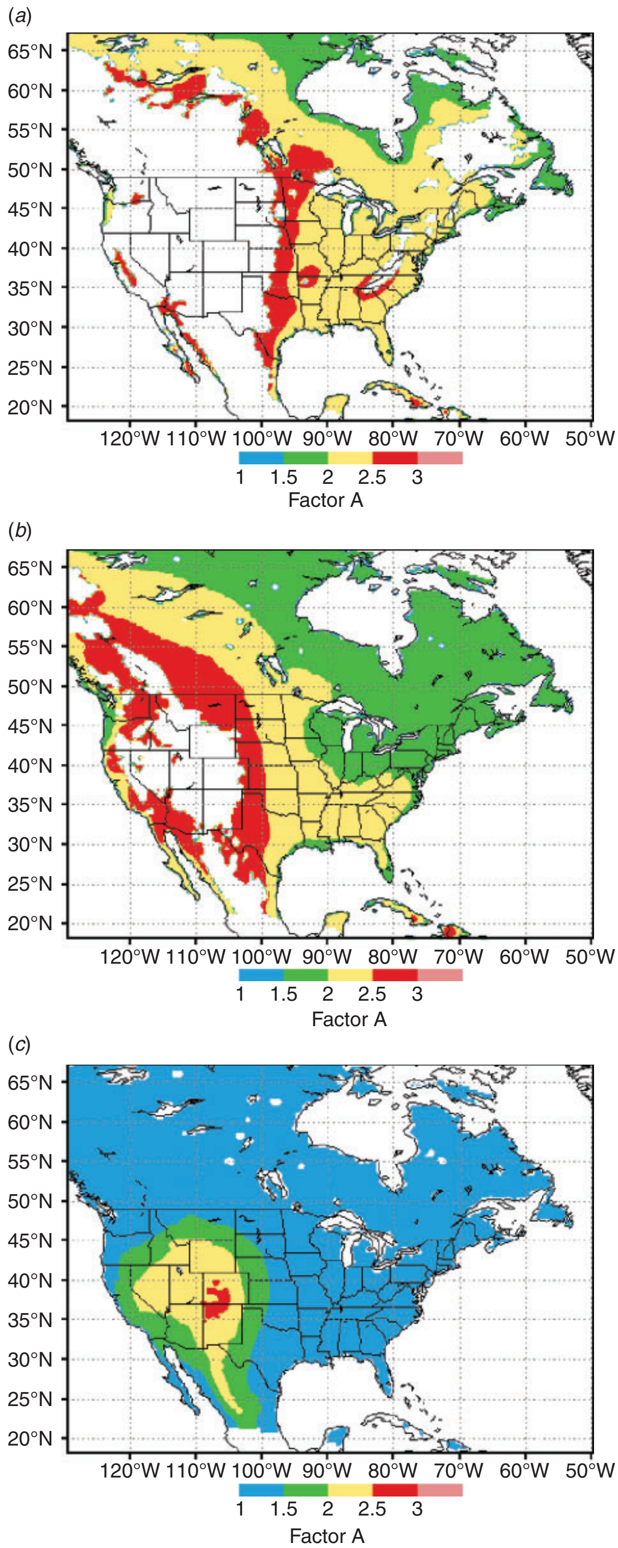

Fig. 2. Warm-season (May to October) mean of the stability factor A during 1980–2007 for: (*a*) the low-elevation variant; (*b*) the mid-elevation variant; and (*c*) the high-elevation variant of the Haines Index. Locations where the surface pressure is less than the higher pressure in the range defined in the caption for Fig. 1 are shown in white.

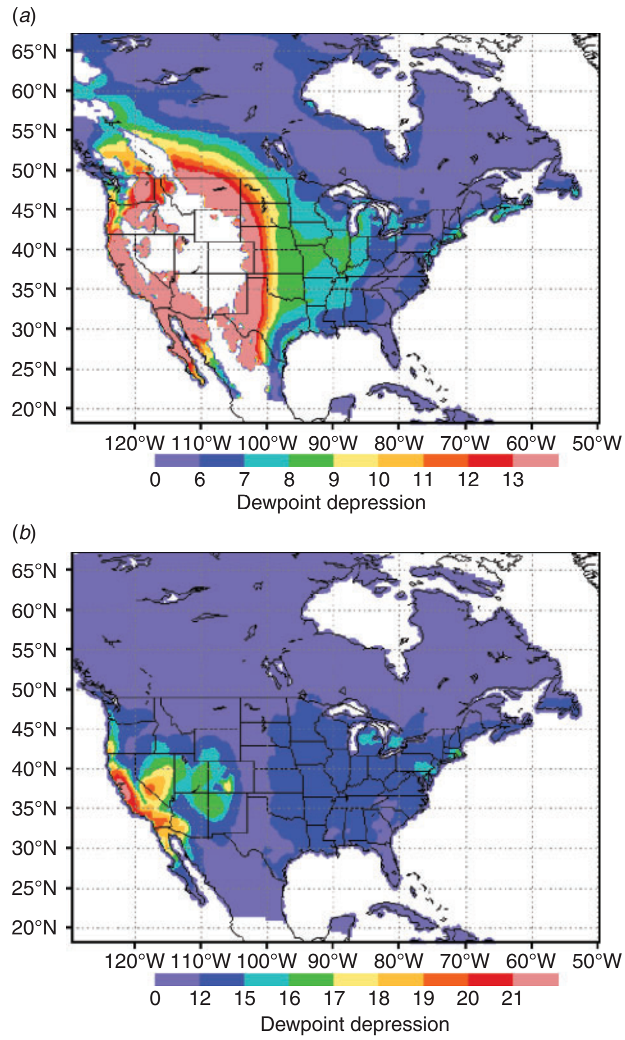

Fig. 3. Warm-season (May to October) mean dewpoint depression (°C) during 1980–2007 for: (*a*) the low- and mid-elevation variant (850-hPa dewpoint depression); and (*b*) the high-elevation variant (700-hPa dewpoint depression) of the Haines Index. Locations where the surface pressure is less than the higher pressure in the range defined in the caption for Fig. 1 are shown in white.

are evident in the comparatively coarse GR climatology. A map of the mean 700-hPa dewpoint depression used in the high-elevation variant (Fig. 3*b*) corresponds more closely to WHC in western North America, with the exception of very fine-scale patches of high values appearing in south-western Nevada and south-central Colorado. Slightly elevated mean 700-hPa dew-point depressions also appear in the north-east United States, where WHC did not present results.

As with factor A, raw factor B values can be 1, 2 or 3 depending on a set range of dewpoint depressions (Table 1). Note that although the low- and mid-elevation variants employ the same 850-hPa dewpoint depression, different ranges are used to calculate factor B for each variant. Spatial variations in factor B for the low- and mid-elevation variants (Fig. 4*a*, *b*) are less evident than those in the 850-hPa mean dewpoint depression

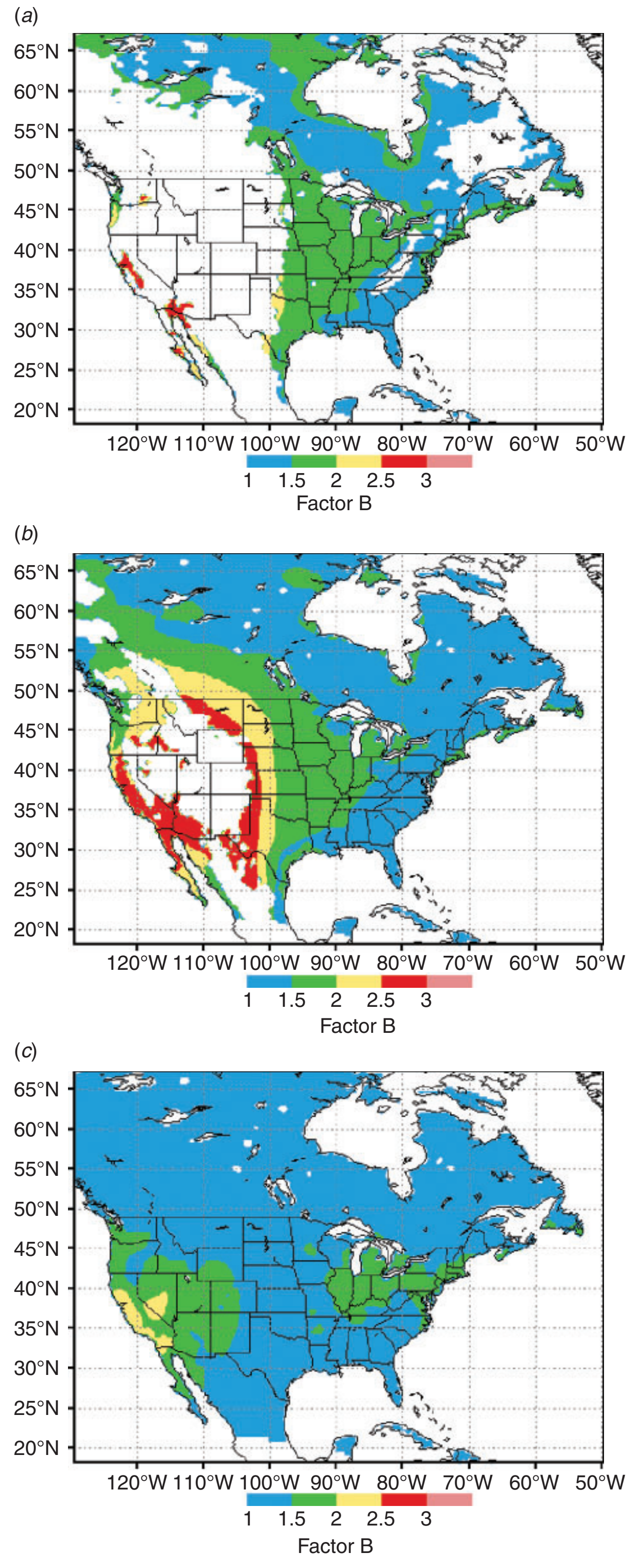

Fig. 4. Warm-season (May to October) mean of the humidity factor B during 1980–2007 for: (*a*) the low-elevation variant; (*b*) the mid-elevation variant; and (*c*) the high-elevation variant of the Haines Index. Locations where the surface pressure is less than the higher pressure in the range defined in the caption for Fig. 1 are shown in white.

maps (Fig. 3*a*) throughout eastern North America. Slightly elevated factor B values appear in the Midwest, corresponding to the location of higher 850-hPa mean dewpoint depressions, but the lobe of higher mean dewpoint depressions along the Iowa–Missouri border into Illinois does not have an evident impact on mean factor B values. The map of high-elevation variant mean factor B (Fig. 4*c*) is also considerably smoother than the corresponding 700-hPa mean dewpoint depression map (Fig. 3*b*), with values exceeding 2 appearing only in southern California and south-western Nevada. Interestingly, the higher mean dewpoint depressions in the north-east appear to yield slightly higher mean factor B values. These results indicate that NARR-based climatological maps of both factor A and factor B exhibit smoother horizontal variations than is evident in maps of the meteorological fields used to calculate each factor, although the smoothing in factor B is also clearly evident even at high elevations, unlike factor A.

Haines Index

The HI is calculated by adding factors A and B with equal weighting at each point to generate an integer value between 2 and 6. As expected from the analyses of the individual components, maps of the warm-season climatological mean HI exhibit more variability and generally higher values in western North America than in the east, owing to higher surface elevations and generally less stable, drier mean conditions (Fig. 5). As seen in the results for factor A and factor B, the NARR-derived HIs are also considerably smoother than expected, considering the comparatively detailed meteorological information that serves as inputs for the computation (cf. Fig. 5 and Figs 1, 3). In fact, the overall patterns are very similar to WHC, in that the large-scale mean values suggest low to moderate values (2–4) in the east, with higher values in the Great Plains and more variability in the high elevations. The NARR values are generally lower than WHC values by ~0.5 in most locations in the low- (Fig. 5*a*) and high-elevation (Fig. 5*c*) variants.

In some locations, the higher spatial resolution of the NARR data produces fine-scale patterns associated with orography and coastlines in the HI maps. The impact of the coastline on the low-elevation mean HI is clearly evident (Fig. 5*a*), whereas lower values of the mean high-elevation variant HI appear in the Central Valley of California (Fig. 5*c*). The more detailed orography in the NARR also permits computation of the mid-elevation variant in California, Oregon and Washington, where mean HI values between 3 and 4 occur in Washington and Oregon, between 4.5 and 5.5 occur in northern and central California, and between 5 and 6 occur in southern California (Fig. 5*b*). Finally, the mid-elevation variant also clearly differentiates between the more maritime climate of western Washington and Oregon, and the arid climate of eastern Washington and north-eastern Oregon, where HI values vary from 3 to 3.5 in the west to 4.5 to 5.5 in the east.

Maps of the standard deviation (s.d.) of the HI are presented in Fig. 6. The s.d. of the low-elevation variant is generally less than 1.0 throughout eastern North America, with particularly small standard deviations evident near the coastline in the south-eastern United States (Fig. 6*a*). This result reveals that HI values in Florida exhibit very little variability in May to October during

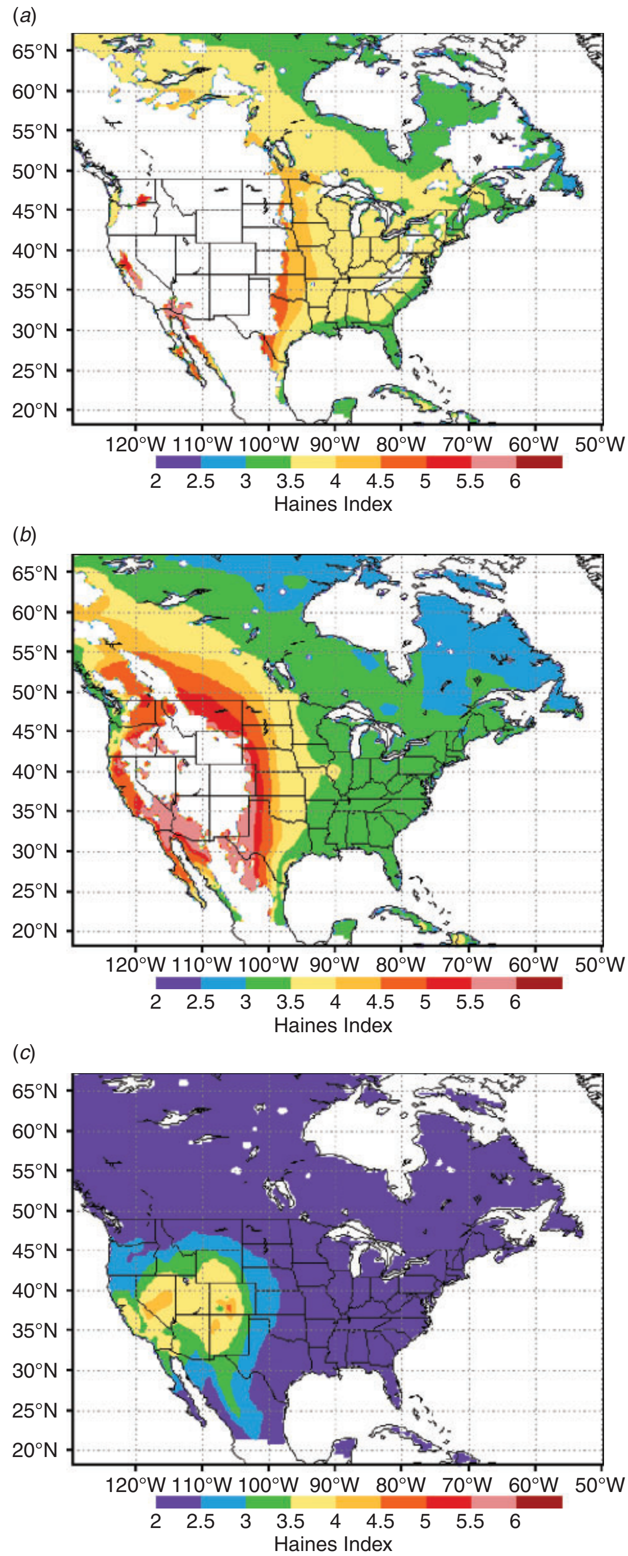

Fig. 5. Warm-season (May to October) mean Haines Index during 1980–2007 for: (*a*) the low-elevation variant; (*b*) the mid-elevation variant; and (*c*) the high-elevation variant. Locations where the surface pressure is less than the higher pressure in the range defined in the caption for Fig. 1 are shown in white.

the 28-year time period of this study, compared with other regions of North America. This information, when combined with the small mean low-elevation variant HI values in Florida (Fig. 5*a*), suggests that the HI values are generally low and remain low from May through October in Florida's generally maritime atmospheric environment. The pattern of s.d. for the mid-elevation variant HI (Fig. 6*b*) is similar to the low-elevation variant, with standard deviations varying between 0.75 and 1 throughout most of the domain. Slightly higher standard deviations occur in the upper Midwest, and lower values occur in Florida and in the Desert Southwest. It is noteworthy, however, that although the mid-elevation variant of the HI is low in Florida with low s.d., in the Desert Southwest, the mean HI is *high* (Fig. 5*b*) with low s.d. So, although the HI is low in Florida and remains low, the HI is exceptionally high in the Desert Southwest and remains high. The s.d. of the high-elevation variant of the HI (Fig. 6*c*) shows similar variability to the other variants in the east, but higher variability (s.d. between 1 and 1.5) in the west, with the highest values reported in a swath across Nevada, Utah, southern Idaho and south-western Montana, and a second area in central New Mexico and along the Mexican high plateau to the south.

Frequency and maximum consecutive days

Maps of the warm-season frequency of HI $\geq$ 4 (Fig. 7*a*, *c*, *d*) and the maximum number of consecutive days in any year of HI $\geq$ 4 (Fig. 7*b*, *d*, *f*) show distributions that are broadly similar to the mean HI maps (Fig. 5), with the highest frequencies and longest sequences occurring in the west, and the lowest frequencies and shortest sequences occurring near the coastlines in the east. As with the mean lapse rate, dewpoint depression and HI maps, the results correspond closely to what was reported in WHC for all three of the HI variants, with the major differences between the NARR and GR maps occurring near the coastline in the eastern USA, and in locations where the WHC did not present the HI owing to the comparatively coarse orography in the GR. Specifically, the NARR maps indicate that frequencies of the low-elevation variant HI $\geq$ 4 (Fig. 7*a*) exceed 60% in western Washington and Oregon and exceed 90% in the valleys of California. However, the maximum number of consecutive days is much shorter in western Washington (~30) than in California (>150) (Fig. 7*b*). A similar pattern in the mid-elevation variant HI $\geq$ 4 is evident in Fig. 7*c*, *d*, with higher frequencies and longer sequences appearing in California than in Washington and Oregon. The high-elevation variant HI $\geq$ 4 frequencies (Fig. 7*e*) show that whereas frequencies greater than 60% appear along the California coastline and in Nevada, frequencies below 60% occur in eastern California. The same pattern appears in the map of high-elevation variant HI $\geq$ 4 maximum consecutive days (Fig. 7*f*), with values greater than 30 in California and Nevada, and values less than 30 in eastern California.

As expected, maps of warm-season frequency (Fig. 8*a*) and maximum consecutive days (Fig. 8*b*) of HI $\geq$ 5 for the low-elevation variant show spatial distributions similar to HI $\geq$ 4, but with lower frequencies and shorter sequences. However, the effect of the coastline in the east is less pronounced than for HI $\geq$ 4 (Fig. 7*a*, *b*). Frequency maps of the mid-elevation variant

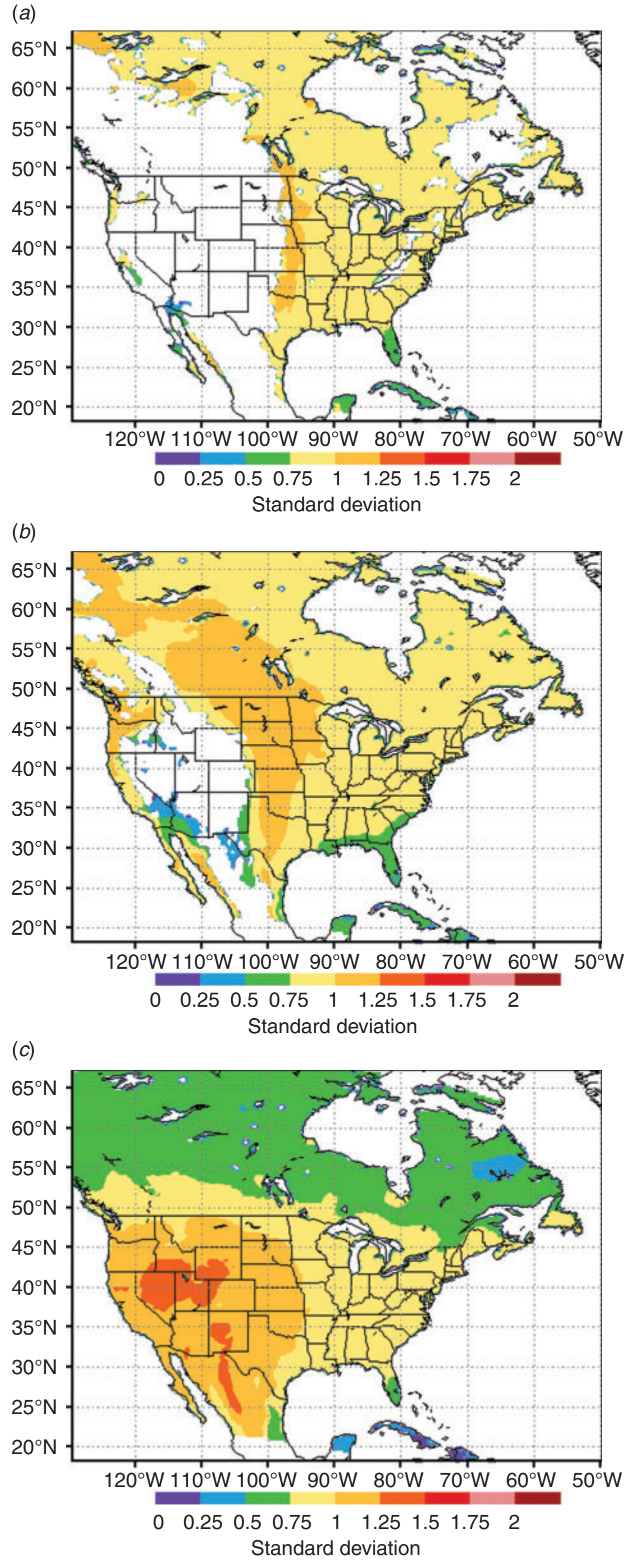

Fig. 6. Warm-season (May to October) standard deviation of the Haines Index during 1980–2007 for: (*a*) the low-elevation variant; (*b*) the mid-elevation variant; and (*c*) the high-elevation variant. Locations where the surface pressure is less than the higher pressure in the range defined in the caption for Fig. 1 are shown in white.

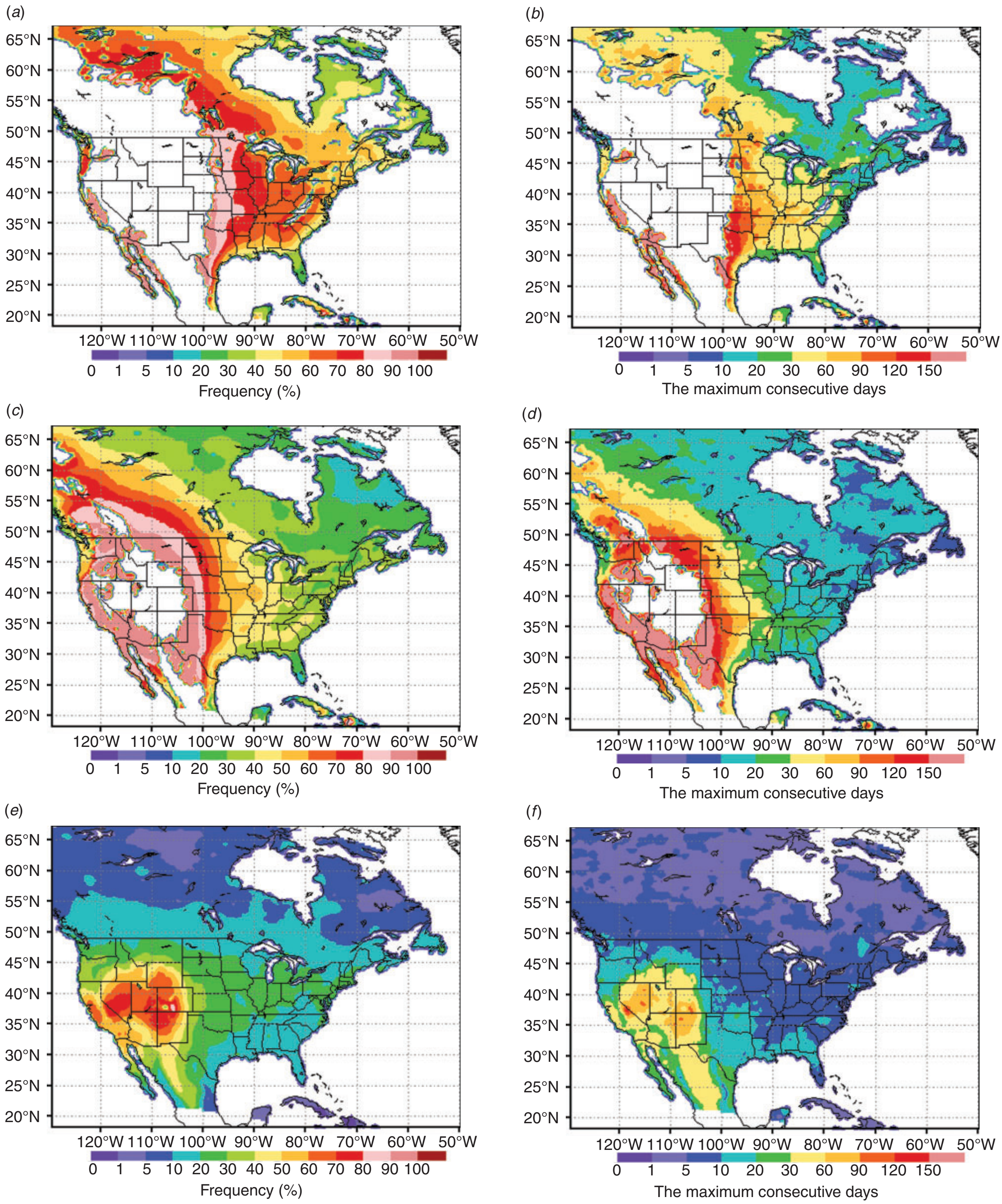

Fig. 7. Haines Index: frequency (as percentage of days per warm season) that the index is ≥4 for: (*a*) the low-elevation variant; (*c*) the mid-elevation variant; (*e*) the high-elevation variant, and the maximum consecutive days with index ≥4 during 1980–2007 for (*b*) the low-elevation variant; (*d*) the mid-elevation variant; and (*f*) the high-elevation variant. Locations where the surface pressure is less than the higher pressure in the range defined in the caption for Fig. 1 are shown in white.

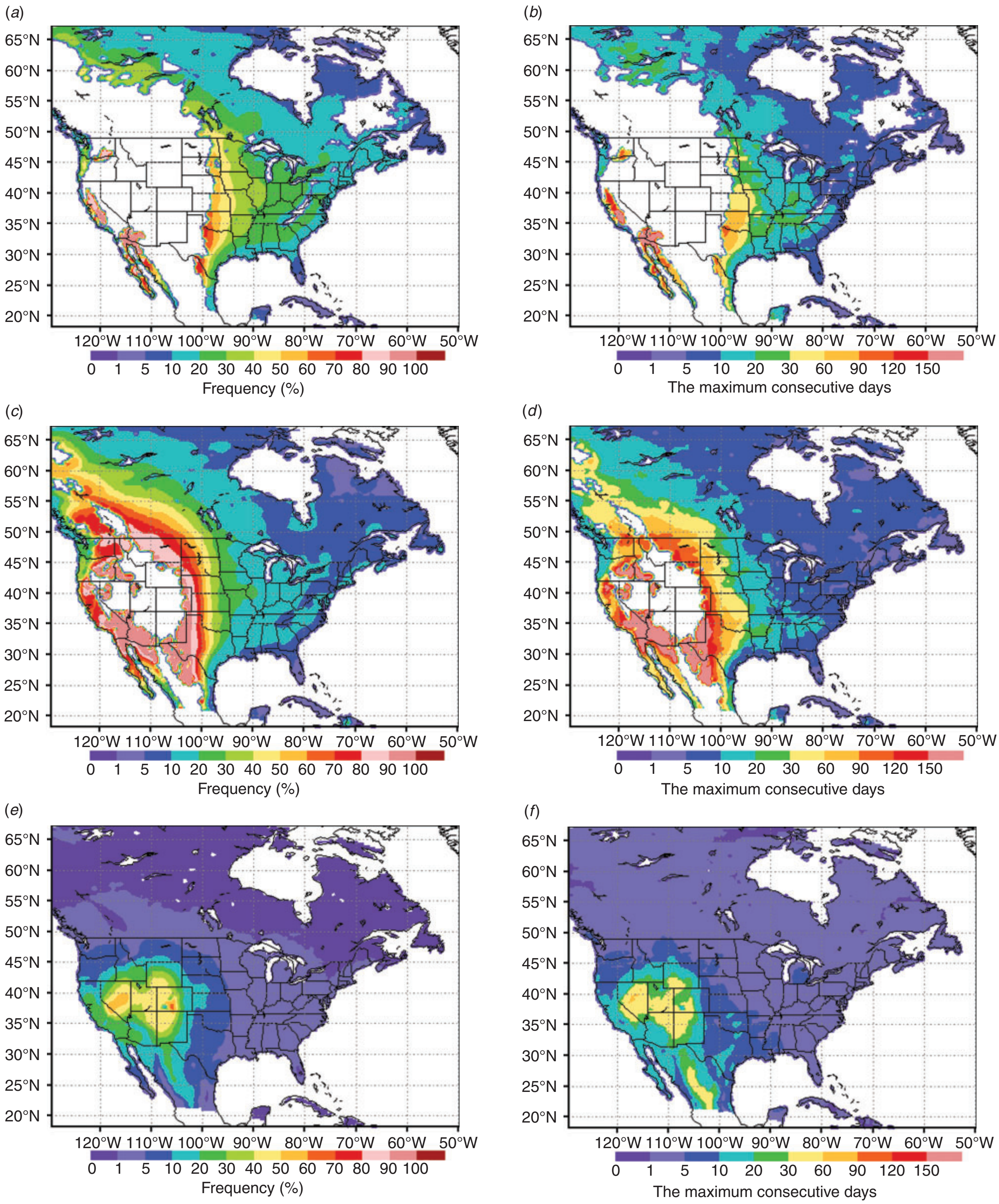

Fig. 8. As in Fig. 7 except for values of Haines Index ≥ 5.

$HI \geq 5$ (Fig. 8*c*), however, highlight differences between northern, central and southern California that are not evident in the $HI \geq 4$ frequency maps (Fig. 7*c*), with $HI \geq 5$ occurring more than 80% of the time in northern and southern California, but less than 70% of the time in central California. Likewise, maximum sequences of $HI \geq 5$ are longer in northern and southern California and shorter in central California (Fig. 8*d*). For the high-elevation variant (Fig. 8*e*), $HI \geq 5$ occurs more

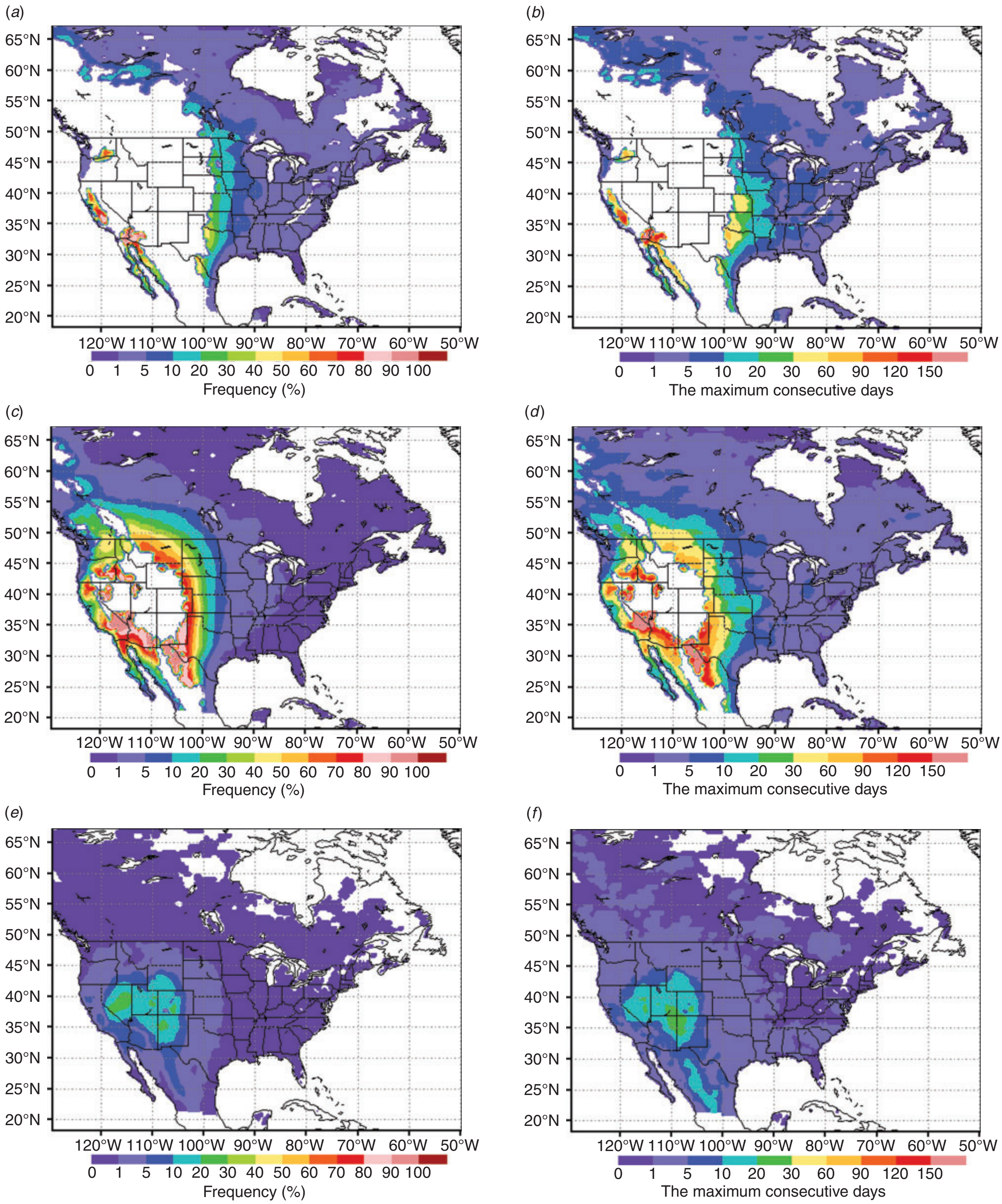

Fig. 9. As in Fig. 7 except for values of Haines Index = 6.

often in central Nevada than in California, in contrast to HI ≥ 4 (Fig. 7*e*), whereas the number of maximum consecutive days of the high-elevation HI ≥ 5 (Fig. 8*f*) is smaller (>20) in California than in Nevada (> 30). For completeness, maps of warm-season frequency and maximum consecutive days of HI = 6 are presented in Fig. 9. These maps show the same spatial variation as Fig. 8 but, as expected, exhibit still smaller frequencies and shorter sequences.

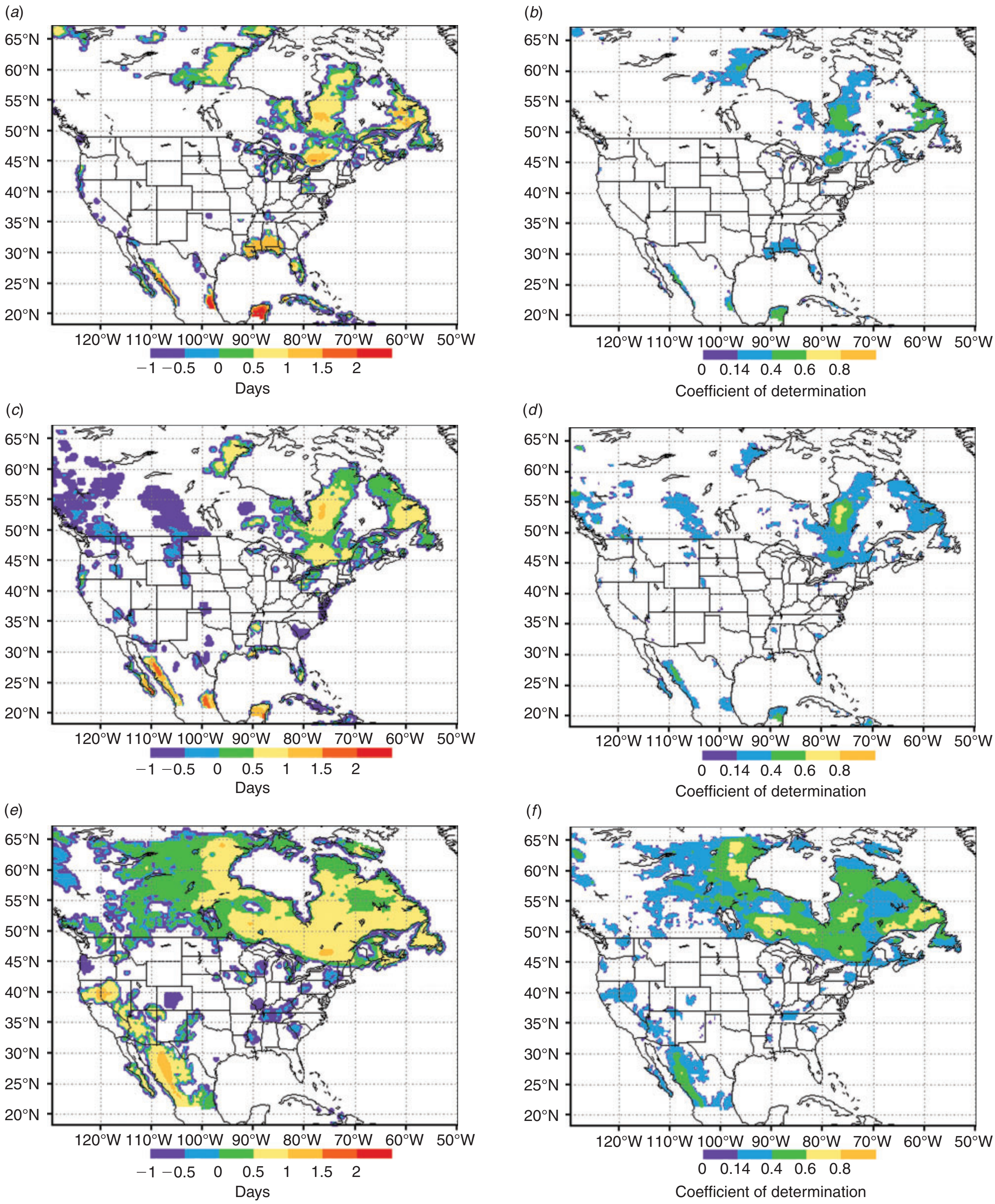

Fig. 10. Map of linear trends in days of Haines Index ≥ 4 for: (*a*) the low-elevation variant; (*c*) the mid-elevation variant; and (*e*) the high-elevation variant. Trends are calculated from time series at each grid cell over the 1980–2007 period. The right column (*b*, *d* and *f*) shows the corresponding coefficient of determination of the linear fit at each grid cell for three elevation variants. Locations with a linear trend $P \leq 0.05$ (level of significance) or where the surface pressure is less than the higher pressure in the range defined in the caption for Fig. 1 are shown in white.

Temporal trends

Temporal trends in the number of days (variable Y) in each year during the 28-year period when HI ≥ 4 are analysed by performing a simple linear regression analysis in time (variable X) for each HI variant at each grid point in the study domain. Fig. 10 shows the spatial distribution of the slope parameter (the B coefficient for variable X) of the regression line ($Y = BX + A$) for HI ≥ 4 along with the coefficient of determination that indicates the fraction of the variances in the time series data (Y) that are accounted for by the variation of independent variable X. A test of the B coefficient was applied for each location and only those with $P \leq 0.05$ were accepted. The linear response of Y to the changes in X is greater (less) when the slope parameter is farther (closer) from (to) zero. The spatial patterns are similar for all three variants. For most regions of the United States, the annual number of days with HI ≥ 4 does not appear to follow an obvious increasing or decreasing trend. For the low- and mid-elevation variants, some areas in the Northeast and the Deep South show a positive trend, whereas only very small isolated areas exhibit a weak negative trend. For the high-elevation variant, areas of positive trend are also found in northern California, the Intermountain West and the Desert Southwest. Positive trends are seen over most of south-east Canada and around the Hudson Bay, whereas negative trends occur in south-west Canada. Overall, the number of days with HI ≥ 4 in each warm season does not show an obvious linear response to time.

Conclusions and recommendations

A climatology of the HI was developed for North America, employing the gridded temperature and humidity fields from 32-km NARR data from 1980 to 2007. Maps of warm-season mean lapse rates, dewpoint depressions, factor As, factor Bs and the HI for each of the low-, mid- and high-elevation variants were computed and compared with the GR-based climatology of WHC. Standard deviations of the HI, frequencies and maximum consecutive days of HI ≥ 4, HI ≥ 5 and HI $= 6$ and temporal trend analyses of days in each year where HI ≥ 4 for each variant were employed to investigate the spatial and temporal variability of the NARR-derived HI climatology across North America. The hypothesis that a more spatially detailed climatology provides additional information that can augment the results from WHC was evaluated.

We found that although the NARR produces spatially detailed meteorological fields, the ranges of lapse rate and dewpoint depressions used to determine factor A and factor B (Table 1) appear to generate smoother resultant HI maps. The result of this smoothing is that, broadly speaking, the NARR HI climatology maps presented here correspond closely to the analogous GR maps presented in WHC, despite the differences in spatial resolution between the NARR and the GR. Therefore, the hypothesis that a HI climatology computed from the NARR will resolve the impact of mesoscale variations in lapse rate and dewpoint depression on the continental and regional distribution of the HI was found to be false for most locations in North America. Exceptions to this result occur near coastlines in eastern North America and near steeply sloping terrain in the west, such as along the California–Nevada and Colorado–New Mexico borders. Furthermore, in locations such as California, Oregon and Washington where NARR-derived HI values for the mid-elevation variant could be computed but the comparatively coarse orography in the GR data precluded presentation of the mid-elevation variant in WHC, this study provides additional climatological information that was not previously available. Finally, a trend analysis showed that over most of the study area, there is no significant linear trend in the total number of high HI days occurring in each warm season over the 28-year data period.

An implication of this study is that the WHC is likely to provide sufficient spatial detail for fire managers and fire weather forecasters to interpret the variability of the HI at most locations in North America. In parts of eastern North America where maritime conditions prevail in the warm season and in areas where steeply sloping terrain is not well resolved in the GR but is resolved in the NARR (e.g. the Pacific Northwest), the NARR climatology presented here can be employed in addition to the GR-based WHC to aid in analysing the performance and interpreting the results of the HI. Additionally, because the NARR climatology presented here computes the HI elevation variants at every location in North America where the pressure levels required for the variant are above the ground, fire managers and fire weather forecasters using the HI at a given location can use this climatology to determine whether more than one elevation variant could provide information about the potential for aboveground atmospheric conditions to impact a plume-dominated fire such that the fire becomes large or exhibits erratic fire behaviour.

Acknowledgements

This research is supported partially by the China Scholarship Council, partially by the National Basic Research Program of China (grant 2009CB421402), partially by the USDA Forest Service Northern Research Station (grant 07-JV-11242300–049) and partially by the USDA Forest Service Pacific Southwest Research Station under the auspices of the Joint Fire Science Program. We also acknowledge the helpful comments and recommendations from two anonymous reviewers.

References

Black TL (1988) The Step-mountain Eta coordinate regional model: a documentation. NOAA/NWS Report. (Camp Springs, MD)

Croft PJ, Watts M, Potter BE (2001) The analysis of the Haines Index climatology for the eastern United States, Alaska, Hawaii, and Puerto Rico. In 'Fourth Symposium on Fire and Forest Meteorology', 12–15 November 2001, Reno, NV. Paper No. 8.7. (American Meteorological Society: Boston, MA)

Haines DA (1988) A lower atmosphere severity index for wildland fires. *National Weather Digest* **13**, 23–27.

Janjić ZI (1994) The step-mountain Eta coordinate model: further developments of the convection, viscous sublayer, and turbulence closure schemes. *Monthly Weather Review* **122**, 927–945. doi:10.1175/1520-0493(1994)122<0927:TSMECM>2.0.CO;2

Jones KM, Maxwell C (1998) A seasonal Haines Index climatology for New Mexico and the significance of its diurnal variations in the elevated Southwest. In 'Preprints, Second Conference on Fire and Forest Meteorology', 11–16 January 1998, Phoenix, AZ, pp. 127–130. (American Meteorological Society)

Kalnay E, Kanamitsu M, Kistler R, Collins W, Deaven D, Gandin L, Iredell M, Saha S, White G, Woollen J, Zhu Y, Chelliah M, Ebisuzaki W, Higgins W, Janowiak J, Mo K, Ropelewski C, Wang J, Leetmaa A, Reynolds R, Jenne R, Joseph D (1996) The NCEP/NCAR 40-year reanalysis project. *Bulletin of the American Meteorological Society* **77**, 437–471. doi:10.1175/1520-0477(1996)077<0437:TNYRP>2.0.CO;2

Kistler R, Kalnay E, Collins W, Saha S, White G, Woollen J, Chelliah M, Ebisuzaki W, Kanamitsu M, Kousky V, van den Dool H, Jenne R, Fiorino M (2001) The NCEP–NCAR 50-year reanalysis: monthly means CD-ROM and documentation. *Bulletin of the American Meteorological Society* **82**, 247–267. doi:10.1175/1520-0477(2001)082<0247:TNNYRM>2.3.CO;2.

McCaw L, Marchetti P, Elliott G, Reader G (2007) Bushfire weather climatology of the Haines Index in south-western Australia. *Australian Meteorological Magazine* **56**, 75–80.

Mesinger F, Janjić ZI, Nickovic S, Gavrilov D, Deaven DG (1988) The step-mountain coordinate – model description and performance for cases of Alpine lee cyclogenesis and for a case of an Appalachian redevelopment. *Monthly Weather Review* **116**, 1493–1518. doi:10.1175/1520-0493(1988)116<1493:TSMCMD>2.0.CO;2

Mesinger F, DiMego G, Kalnay E, Mitchell K, Shafran PC, Ebisuzaki W, Jovic D, Woollen J, Rogers E, Berbery EH, Ek MB, Fan Y, Grumbine R, Higgins W, Li H, Lin Y, Manikin G, Parrish D, Shi W (2006) North American regional reanalysis. *Bulletin of the American Meteorological Society* **87**, 343–360. doi:10.1175/BAMS-87-3-343

Potter BE, Martin JE (2001) Accuracy of 24- and 48-hour forecasts of Haines' Index. *National Weather Digest* **25**, 38–46.

Potter BE, Borsum D, Haines DA (2002) Keeping Haines real – or really changing Haines? *Fire Management Today* **62**, 41–46.

Potter BE, Winkler JA, Wilhelm DF, Shadbolt RP (2005) Computation of the low-elevation Haines Index. In 'Sixth Fire and Forest Meteorology Symposium/19th Interior West Fire Council Meeting', 25–27 October 2005, Canmore, AB, Canada. Paper No. P1.3. (American Meteorological Society: Boston, MA)

Werth J, Werth P (1998) Haines index climatology for the western united states. *Fire Management Notes* **58**, 8–17.

Winkler JA, Potter BE, Wilhelm DF, Shadbolt RP, Piromsopa K, Bian XD (2007) Climatological and statistical characteristics of the Haines Index for North America. *International Journal of Wildland Fire* **16**, 139–152. doi:10.1071/WF06086

Manuscript received 3 December 2008, accepted 27 May 2010